Tellus (2001), 53B, 441–461
Printed in UK. All rights reserved

TELLUS
ISSN 0280–6509

Effects of continental boundary layer evolution, convection, turbulence and entrainment, on aerosol formation

By E. D. NILSSON*[1], Ü. RANNIK[2], M. KULMALA[2], G. BUZORIUS[2] and C. D. O'DOWD[2,3],
[1]*Department of Meteorology, Stockholm University, S-10691 Stockholm, Sweden;* [2]*Department of Physics, P.O. Box 9, FIN-00014 University of Helsinki, Finland;* [3]*Also at Department of Physics, National University of Ireland, Galway, Ireland*

(Manuscript received 22 June 2000; in final form 26 March 2001)

ABSTRACT

Aerosol nucleation events occurring in the continental boundary layer over the boreal forest region in Finland, during the BIOFOR experiment, have been examined to elucidate the rôle of micrometeorology in promoting such events. Invariably, during the spring campaign of 1999, nucleation events occurred in Arctic and polar air masses during cold air outbreaks. Under clear-sky conditions, typical of these synoptic meteorological patterns, the boundary layer evolution was characterized by the rapid growth of a mixed layer, convection and strong entrainment, first from the residual later and later from the free troposphere. It was found that the freshly nucleated particles were detected within two hours from the onset of strong turbulent kinetic energy, independent of how fast the boundary layer evolved. When considering the growth time from cluster size of ≈ 1 nm to detectable sizes of 3 nm, the nucleation and onset of strong turbulence coincided almost exactly. The most likely site for nucleation to take place was the mixed layer or the entrainment zone, while the forest canopy and the free troposphere could be excluded as the nucleation region. There are several possible explanations for the correlation between the onset of turbulence and nucleation: (1) new aerosols or clusters may have been entrained from the residual layer into the mixed layer where they then (in the case of clusters) underwent growth to detectable sizes; (2) two or more precursor gases may have been mixed with each other over the entrainment zone; (3) the adiabatic cooling in the rising convective plumes and the turbulent fluctuation in temperature and vapors by the entrainment flux may have enhanced aerosol formation; (4) a sudden decrease in preexisting aerosol due to dilution of the mixed layer aerosol by entrained air may have reduced the vapor sink enough to initiate nucleation. However, the lack of vertical profile measurements of nucleation mode aerosols, precursor vapors and turbulent fluctuations throughout and above the mixed-layer results in it remaining an open question as to which one of these processes dominates.

1. Introduction

The formation of particles, detected at >3 nm diameter, and subsequent growth to ~ 100 nm in 1–2 days, has in recent years been observed frequently in the continental boundary layer at several European sites. The observations span from sub-arctic Lapland, over the remote boreal forest (Mäkelä et al., 1997; Kulmala et al., 1998b), suburban Helsinki (Väkevä et al., 2000), industrialized agricultural regions in Germany (Birmilli and Wiedensohler, 2000), a mountain site in southern Germany (Birmilli et al., 2000) to rural United Kingdom (Coe et al., 2000).

In an effort to elucidate the processes leading to aerosol nucleation and growth over the boreal forest, a dedicated project Biogenic Aerosol

* Corresponding author.
e-mail: dolan@misu.se.se

Formation Over the Boreal Forest (BIOFOR) was conducted over a two-year period from 1998–1999 (for an overview, see Kulmala et al. (2001a)).

Three campaigns took place in Hyytiälä (61°51′N 24°17′E) in the boreal forest of central southern Finland: BIOFOR 1 from 11 April to 22 May in 1998, BIOFOR 2 from 17 July to 29 August in 1998, and BIOFOR 3 from 11 March to 30 April in 1999. Hyytiälä is also the site for the Finnish SMEAR II station (Station for Measuring forest Ecosystem-Atmospheric Relations) with continuous long term monitoring of, for instance turbulent fluxes and aerosol physics, which allow us to place BIOFOR results into a context of annual cycles and inter annual variability. BIOFOR 1 and 3 were scheduled to coincide with the spring maximum of nucleation event frequency-of-occurrence, while BIOFOR 2 coincided with the summer minimum.

The most studied and best understood atmospheric nucleation mechanisms are binary homogeneous nucleation by H_2SO_4 and H_2O (Kulmala et al., 1998) and ternary nucleation by H_2O, NH_3 and H_2SO_4 (Korhonen et al., 1999). In summary, binary nucleation can occur under low temperature and low aerosol condensation sink conditions, while ternary nucleation is predicted to occur more frequently under warmer conditions. It was, however, also found that meteorological processes could also enhance the nucleation probability under conditions where the mean precursor concentrations were insufficient to trigger nucleation. For example, Easter and Peters (1994) or Pirjola et al. (2000) found that turbulent fluctuations and boundary layer circulation could enhance predicted nucleation rates, while Nilsson and Kulmala (1998) revealed nucleation enhancement due to effect of mixing across a temperature and humidity gradient (e.g., over a capping inversion). Nilsson et al. (2000) also illustrated that atmospheric waves will promote aerosol nucleation. All the above studies found that the nucleation rate could be enhanced several orders of magnitude, compared to the nucleation rate at mean temperature and average vapor concentrations, due to the large sensitivity of the nucleation process on fine scale temporal and spatial variability in meteorological and precursors parameters. Recently, De Reus et al. (1998) and Zahn et al. (2000) found support in flight measurements for nucleation caused by mixing across the tropopause while studies by Mäkelä et al. (1997), Kulmala et al. (1998), Birmilli and Wiedensohler (2000), and Väkevä et al. (2000) have found evidence eluding to a connection between aerosol nucleation and boundary layer dynamics.

In terms of nucleating species, BIOFOR was specifically designed to examine the role of the oxidation products of monoterpenes and/or other organic compounds emitted from the forest, in nucleating new particles in this environment. Buzorious et al. (2001), however, could not find a connection between the photosynthetic activity of the forest and aerosol formation events and therefore, no support for a link between biogenic emissions of precursor gases and nucleation and condensation processes could be found.

Furthermore, Jansson et al. (2001) was unable to find any support for a connection between nucleation and the oxidation products from monoterpenes by reaction with OH, O_3 or NO_3. On the other hand, NH_3 concentrations, together with the calculated H_2SO_4 source term, illustrated some correlation with the maximum number concentration achieved during particle events, particularly when the preexisting aerosol surface was taken into consideration. While these findings can not rule out biogenic organics in the nucleation processes, they suggest that ternary nucleation of H_2O, NH_3 and H_2SO_4 could also account for the observed aerosol nucleation (Korhonen et al., 1999; Kulmala et al., 2000). This is further supported by model simulations specific to case studies during BIOFOR (Kulmala et al., 2001b); however, this particular study does not focus on the chemical mechanisms leading to nucleation, but instead, the role of micro-meteorological processes in promoting nucleation is examined.

Influences of large scale meteorology were examined in an associated paper by Nilsson et al. (2001) who found a link between the synoptic weather and air mass types to aerosol nucleation. Nucleation days were always during Arctic or Polar air masses, cold air advection and cold air outbreaks behind the cold fronts of the cyclonic waves on the Arctic or Polar fronts. Nilsson et al. (2001) pointed to the need to understand what dynamic boundary layer processes are involved in nucleation events and on the spatial scale between the microscale of aerosol dynamics and the scale of synoptic weather systems. Building on the observed connection between synoptics and nucle-

ation, BIOFOR data are examined with particular focus on boundary layer characteristics associated with the observed nucleation events over.

2. Experimental

2.1. SODAR

A Sensitron AB monostatic 2.3 kHz doppler SODAR system (Sound Detection and Ranging) was used to measure the stability of the air (echo strength) and mean and standard deviation of the horizontal and vertical wind components as well as wind direction up to 500 m in 25 m intervals. In practice, the range varied with the stability: at high stability, very little echo returned from above 100 m, which limited the range in which air motions could be calculated, while under unstable conditions, sufficient echo was returned from 200 m or more above the surface. Raw echo measurements were achieved in 8-s cycles between the three antennas. The vertical antenna echo strength was averaged and stored every 3 min. Wind averages and standard deviations was derived and averaged over 30 min periods.

2.2. Eddy covariance system

Turbulent fluxes were measured in the mast in Hyytiälä above a 14-m high Scots pine forest by two eddy covariance systems at 23.3 and 46.0 m above the forest floor. The eddy covariance system consisted of an ultrasonic anemometer (Solent Research R3, GILL, UK) which measures three wind speed components and sonic temperature at 21 Hz, an infrared gas analyzer (LI 6262, Li-Cor, USA) for H_2O and CO_2 measurements with the instrumental first-order response time of 0.1 s, and at 23.3 m, a condensation particle counter (CPC TCI 3010) with a first-order response time of about 0.8 s was deployed. Teflon (7 m long) and stainless steel (4.5 m long) lines were used to bring the sample air from close to the anemometer into instrumental boxes of the gas analyzer and CPC, respectively, located on the mast. The 30 min average fluxes of heat, CO_2, H_2O and particles were calculated as the co-variances between the concentrations (or temperature) and vertical wind speed with respect the flow streamlines. The fluxes were calculated and corrected for underestimation as described by Aubinet et al. (2000). About 50% of particles with diameter 14 nm were detected by the particle eddy covariance system. The combined effect of CPC detection efficiency and diffusion losses in the sampling line on particle detection was determined by laboratory calibration as described by Buzorius (2000). Therefore, the calculated particle number flux includes the sizes about 10 nm and bigger in diameter. For more details on the eddy covariance system and measurements during BIOFOR, see Buzorius et al. (2001).

2.3. Soundings

To follow changes in the boundary layer structure during the BIOFOR field campaigns, we performed a series of radiosoundings using the Vaisala sounding systems. Sondes where launched on a regular basis by the Finnish Meteorological Institute (FMI) from Jokioinen (60°49′N 23°30′E, 104 m a.s.l., 179 km southwest of Hyytiälä) at 0 and 12 UTC and from Tikkakoski (62°24′N 25°40′E, 141 m a.s.l., 93 km northeast of Hyytiälä) at 6 and 18 UTC. At Hyytiälä soundings were made during part of BIOFOR 1 (20 sondes) and most of BIOFOR 3 (41 sondes) campaigns in collaboration with the Finnish Army. A more technical description of the soundings is given in Nilsson et al. (2001).

2.4. Aerosol measurements

The dry aerosol number size distributions were measured with a Differential Mobility Particle Sizer (DMPS) system in 10 minutes cycles at 2, 18 and 67 m heights in Hyytiälä, resulting in a pseudo-continuous characterization of the size distribution and the evolution of sub micrometer aerosol particles. The DMPS system used comprised two DMPS systems: the first DMPS coupled a TSI 3025 UFCPC to a Hauke-type short DMA (Differential Mobility Analyzer) and measured particles from 3 to 20 nm "dry" diameter. The second system coupled a TSI 3010 CPC to a medium-length Hauke-type DMA and measured particles from 20 to 500 nm. Aalto et al. (2001) reports more details of this system, together with the other aerosol physical measurements.

Nucleation events were classified according to DMPS spectral shape and evolution and clarity of the events and are discussed in Mäkelä et al. (2000) and Kulmala et al. (2001). In this analysis,

the two most clear event categories are analyzed for links to boundary layer dynamics using only the ground based DMPS system which sampled air from 2 m height above the forest floor.

3. Results

3.1. Diurnal evolution of the boundary layer

All clear nucleation event days were associated with cold air advection and occurred behind the cold front of a cyclonic system in polar and Arctic air masses. Cold air advection is associated with low amounts of medium and high level clouds and only fractional low level cloud-cover. The nucleation days had, on average, half the cloud-cover relative to non-nucleation days (Nilsson et al., 2001). This resulted in a higher incoming solar radiation flux, a higher net surface radiation during daytime, and a negative net radiation during nighttime. The incoming solar radiation increased more rapidly in the morning, and the maximum solar flux at noon was, on average, a factor two larger than on non-nucleation days, c.f. Kulmala et al. (1998) or Birmilli and Wiedensohler (2000). While several nucleation studies have considered the effect of enhanced radiation on photochemistry (e.g., enhanced OH radical production leading to enhanced H_2SO_4 production) associated with sunny days (O'Dowd et al., 1999), meteorological aspects have usually been neglected. Not only is incoming solar radiation an important factor in producing nucleation precursors, it is also the most important energy source for turbulence and convection in the boundary layer. The larger amplitude of the diurnal cycle of radiation on a clear-sky day will cause a very different boundary layer compared to a cloudy day with much more turbulent mixing in the former case. Additionally, cold air advection favors unstable stratification, thus further enhancing mixing processes.

Owing to large radiative cooling at the surface, a nocturnal stable boundary layer should form after sunset (Fig. 1) and persist throughout the night. This behavior during the BIOFOR nucleation events is corroborated by in-situ data and illustrated in Fig. 2 for 4 April 1999. This sequence of radio soundings launched at Hyytiälä was conducted during a nucleation day. The first sond was launched before sunrise shows clearly a surface inversion and a stable nocturnal layer up to about 320 m. Above the stable layer there was a residual layer up to 1440 m. If the night was windy or cloudy the stability may be weaken or there may be a shallow mixed layer near surface at night.

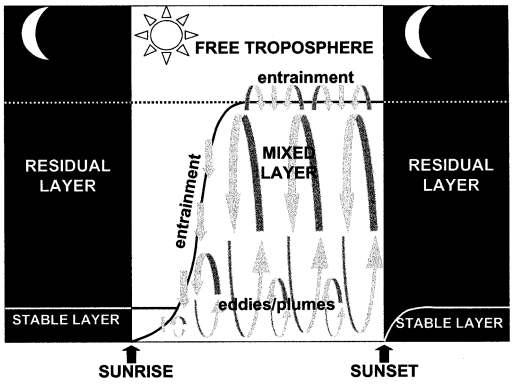

Fig. 1. Schematic figure of the clear sky continental boundary layer diurnal cycle. Black fields represent night, white represent day. Full or dotted lines represent layer interfaces. Black arrows mark sunrise and sunset. Gray downward arrows represent entrainment and gray curved arrows represent convective and turbulent eddies and plumes.

After sunrise, a mixed layer will begin to form near surface as the sun starts to heat the surface and subsequently the near-surface air. In the early morning, this mixed layer grows slowly until it has consumed the remnants of the stable layer. The next sond in Fig. 2 was launched after sunrise and one can clearly see that the temperature profile near surface now had become dry adiabatic, or even slightly super adiabatic. A shallow mixed layer had grown up to 410 m, best seen as the layer of almost constant virtual potential temperature profile between the surface and 410 m. Above this layer a part of the old stable layer still persisted.

By the third sounding, the nocturnal stable boundary layer had disappeared entirely, the boundary layer air had warmed up considerably and the mixed layer extended up to 1640 m. The temperature profile was adiabatic or superadiabatic up to the same height, which indicates convection. This indicates that when the remnants of the nocturnal stable layer have been consumed, the mixed layer height grows rapidly by entrainment of air from the residual layer as turbulent eddies and convective plumes increase their

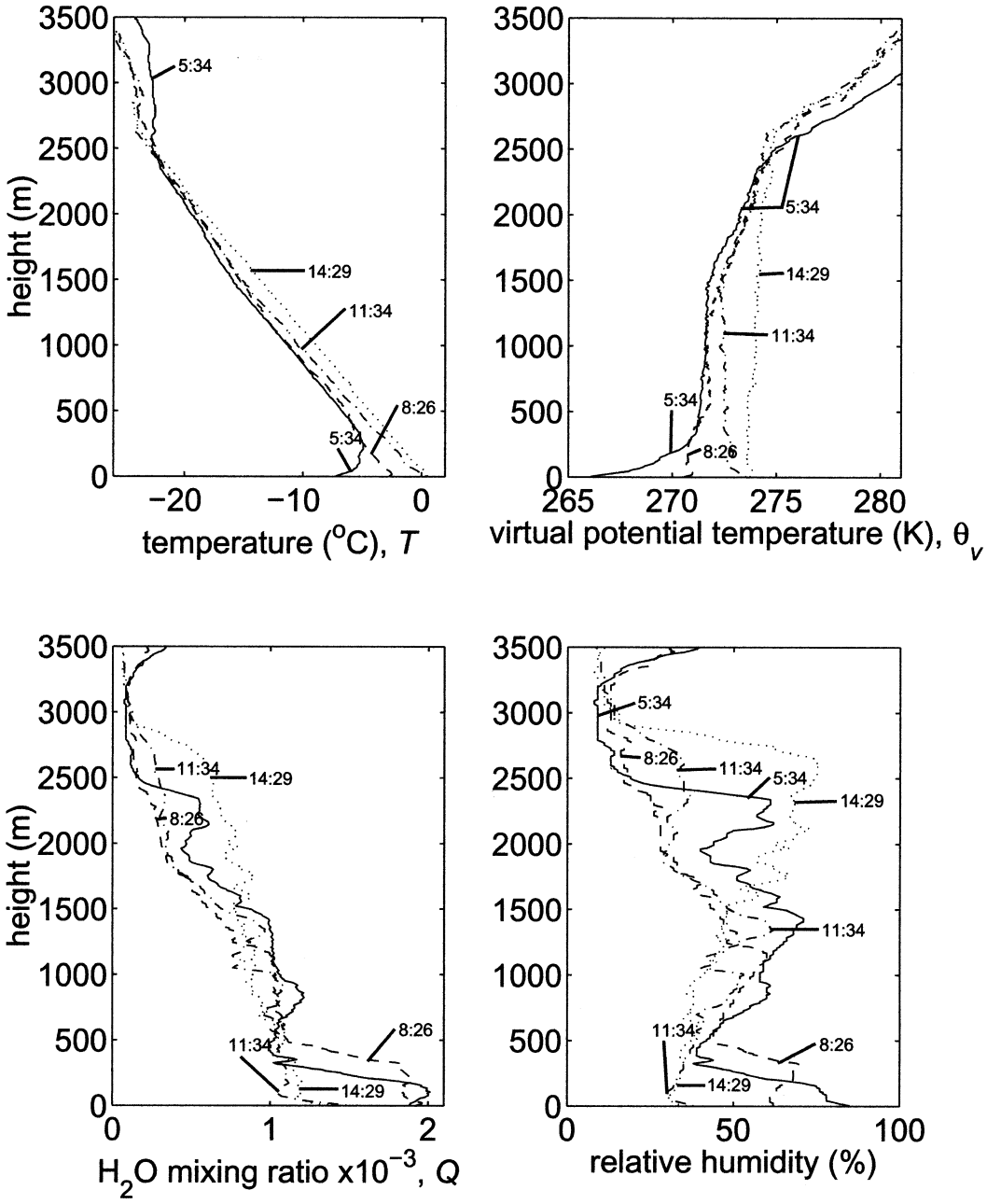

Fig. 2. Temperature, virtual potential temperature, water vapor mixing ratio and relative humidity by height from four radiosondes launched in Hyytiälä on 4 April 1999, during BIOFOR 3.

strength and dept. Typically, at noon, the growth decades as the boundary layer approach its maximum height. Entrainment can mainly result from convective plumes which overshoot the inversion into the stably-stratified or near-neutral air aloft, and which then return undiluted, but bringing with them downdrafts of air, which is effectively mixed into the turbulent mixed layer air. Shear generated mechanical turbulence may contribute to the entrainment. During the growth period of the mixed layer, the entrainment flux will take place from the residual layer. Entrainment will continue into the afternoon, but by then, from the free troposphere. At this stage, the mixed layer growth is small and largely balanced by subsidence and divergence. As the sun sets, convection and turbulence decay rapidly, leaving a new residual layer, and a new stable boundary layer forming near the surface.

The water vapor mixing ratio initially had a large gradient near the top of the nocturnal stable boundary layer, but by this time, the water vapor had been distributed throughout the mixed layer and the largest vertical gradient was now at the mixed layer top between the interface of the moist boundary layer and the dry free troposphere. The relative humidity increased from the surface and up because of the adiabatic cooling in rising convective plumes and reached a maximum around the mixed layer top, still sub-saturated. The warming by solar heating of the surface and the growth of the mixed layer by convection and entrainment continued in the afternoon, and by the last sond at 14:29, the mixed layer height had increased to 2180 m. The air remained sub-saturated, but this does not rule out the possibility of a partial cloud cover of patchy cumulus clouds since the sond is just a point measurement. In fact, cumulus clouds, organized in cloud streets by roll vortices, were observed the same afternoon on satellite images over southern Finland (Nilsson et al., 2001). The boundary layer behaved in a similar manner on all nucleation days, although with some variations, which are discussed below.

The mixed layer warms and grows in dept mainly due to energy input from the surface, however, turbulent entrainment from above the mixed layer also contributes to the growth. Overshooting convective cells, in turn, driven by the surface solar heating, also drives the entrainment flux. Turbulent entrainment leads to stronger temperature inversions at the mixed layer top and, consequently, limits the entrainment rate. Thus, simple mixed layer thermodynamics can explain most of the variation observed in the mixed layer height. Thermodynamics of considering an idealized mixed layer can be presented as

$$z_i \frac{\mathrm{d}\overline{\theta}_{\mathrm{ML}}}{\mathrm{d}t} = \overline{w'\theta'_0} - w'\theta'(z_i), \tag{1}$$

where z_i is the mixed layer height, $\overline{\theta}_{\mathrm{ML}}$ the mixed layer potential temperature, and $\overline{w'\theta'_0}$ and $\overline{w'\theta'}(z_i)$ the heat fluxes at the surface and the mixed layer top. When neglecting large-scale vertical motion, the rate of change of mixed layer height equals to entrainment velocity $\mathrm{d}z_i/\mathrm{d}t = w_{\mathrm{e}}$. In the bulk mixed layer context (Stull, 1988), where the entrainment zone is presented as an infinitesimally thin layer with discontinuous changes in potential temperature and other properties, $\overline{w'\theta'}(z_i)$ can be presented as $\overline{w'\theta'}(z_i) = -w_{\mathrm{e}}\Delta_{\mathrm{EZ}}\overline{\theta}$, where $\Delta_{\mathrm{EZ}}\overline{\theta}$ is the temperature change over the entrainment zone. The evolution of the temperature jump can be predicted as

$$\frac{\mathrm{d}\Delta_{\mathrm{EZ}}\overline{\theta}}{\mathrm{d}t} = \gamma w_{\mathrm{e}} - \frac{\mathrm{d}\overline{\theta}_{\mathrm{ML}}}{\mathrm{d}t}, \tag{2}$$

where γ is the vertical potential temperature gradient just above the entrainment zone. By using an additional closure assumption for the heat flux at the mixed layer top (referred to as energetic method in Stull, 1988), and solving the system of equations, the mixed layer time evolution can be predicted from a potential temperature profile and surface heat fluxes.

Fig. 3 presents the modeled time evolution of mixed layer height and entrainment velocity on 4 April 1999. The mixed layer height is predicted according to potential temperature profile measured at 08:26 as illustrated in Fig. 2. The bulk model predicts fast mixed layer growth until it has reached the top of the residual layer. After that, slower mixed layer growth continues owing to the entrainment from the free troposphere. During the growth through the residual layer, high entrainment velocities (up to 1.5 ms^{-1}) were predicted. Good correspondence of the mixed layer height with those determined from later soundings gives confidence in the ability of the relatively simple bulk mixed layer model to predict, with a good degree of accuracy, the mixed layer evolution between two soundings.

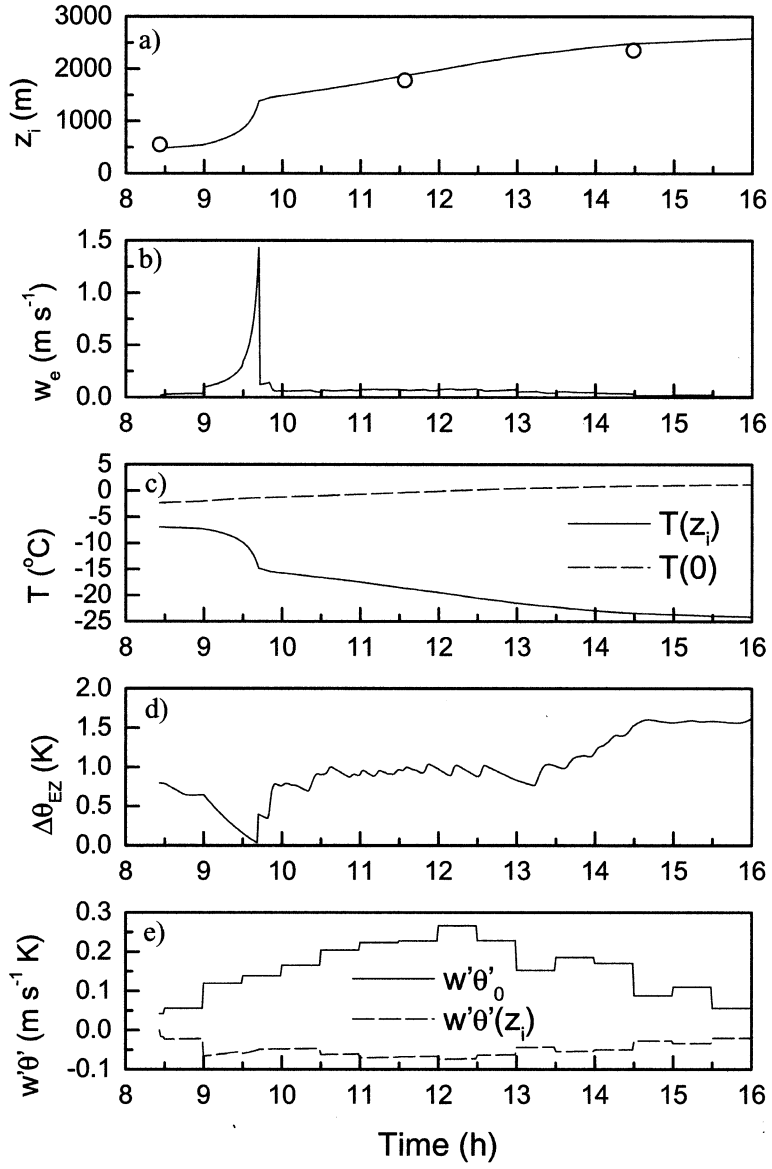

Fig. 3. (a) Thermodynamic simulation (full lines), with energetic method closure, of the mixed layer growth for Hyytiälä on 4 April 1999. Circles represents observed mixed layer heights. (b) The entrainment velocity. (c) The temperature at surface (dashed line) and mixed layer top (full line). (d) The temperature difference over the entrainment zone. (e) The turbulent sensible heat flux at the surface (full line, observations) and at the mixed layer top (dashed line).

3.2. Time of start of nucleation events

Fig. 4 illustrates a good example of aerosol and turbulent characteristics on a typical nucleation day. Fig. 4a shows both the SODAR echo (isopleth lines with the highest values near surface) and the vertical wind variance (σ_w), which is proportional to the vertical component of the turbulent kinetic energy, from 4 April 1999 (BIOFOR 3). At night, and for a while after the sunrise, large echoes were received from near surface due to the surface inversion seen in the first sond in Fig. 2, and σ_w

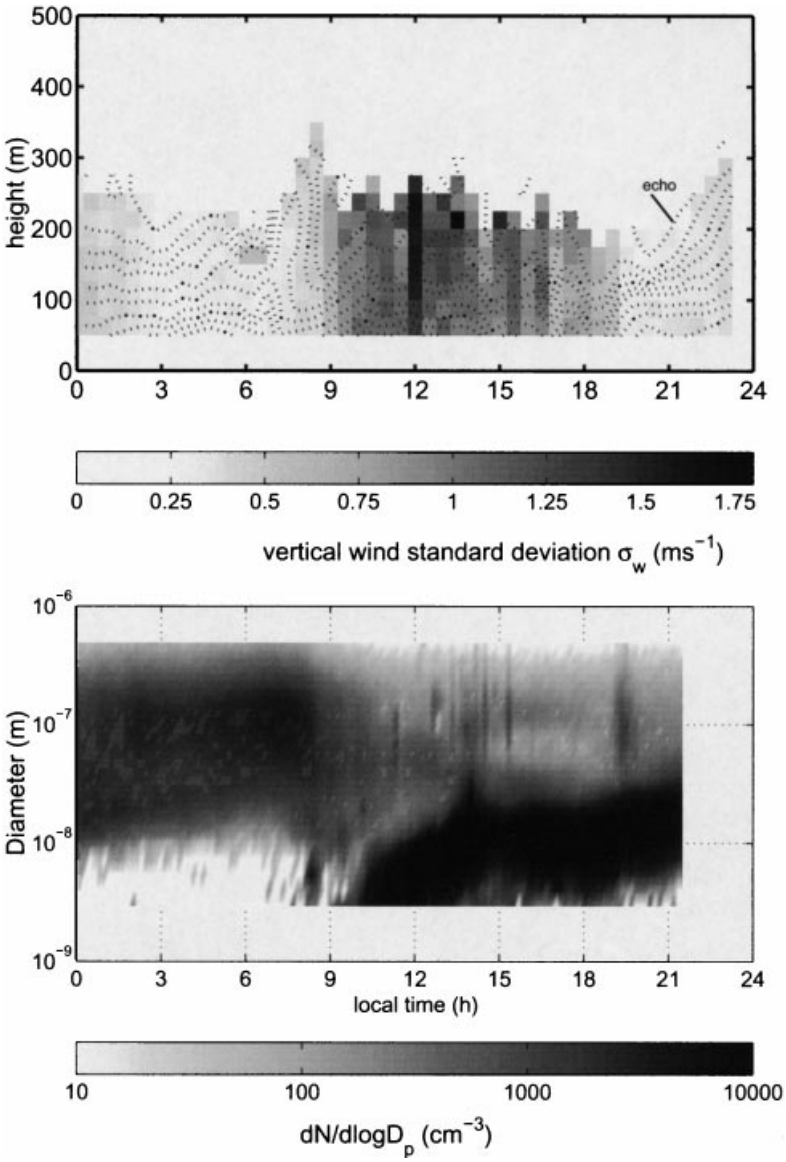

Fig. 4. (a) Echo (dotted isopleth lines) and vertical wind standard deviation (grayscale) as measured by the SODAR on 4 April 1999 (BIOFOR 3). (b) Aerosol number size distribution from the DMPS system at 2 m height.

was small. By about 7–8:30, one can see in Fig. 4a how a strain of echo from aloft appears as a new shallow mixed layer form below the inversion. The surface inversion "lifts", as seen in the second sond of Fig. 2. From now on, the strong echoes near surface are due to thermal convective plumes. At about 9:00 local time, when the lifted inversion gets out of reach of the SODAR, there is a dramatically increase in turbulent kinetic energy throughout the lowest 250 m, coinciding with period of largest w_e and fastest mixed layer growth in Fig. 3. It appears that the increase in turbulent kinetic energy in Fig. 4a were caused by the strong turbulence and convection associated with the

period of fast growth of the mixed layer height after the break up of the nocturnal stable layer when entrainment fluxes also reached their largest values. It can be seen in Fig. 4b that on the same day, the number concentration at the lower DMPS size detection limit, 3 nm, increased rapidly, at about 9:10 local time, indicating that aerosol nucleation was taking place or recently had taken place. Considering that the new particles or clusters probably are 1 nm or less in diameter when they initially form, the nucleation should have started slightly before the 3 nm particles were observed.

It appears from Fig. 4, that the onset of strong turbulent kinetic energy and nucleation appears at the same time. This could be a coincident. However, the case in Fig. 4 only exemplifies a more general observation. It appears that on all nucleation days during BIOFOR, the nucleation was observed 10 min to 2 h after the onset of the convection, strong turbulence and entrainment, typically in the late morning, but sometimes earlier and sometimes later.

Fig. 5 shows the relationship between the onset of strong turbulence, t_{turb} as seen by the SODAR, and the observation of 3 nm particles, $t_{3\,\mathrm{nm}}$, for all clear nucleation cases when both SODAR and DMPS data were available. The appearance of 3 nm particles was always observed after the onset of strong turbulence. This agrees with Väkevä et al. (2000) who also observed nucleation in association with the rapid growth of the mixed layer in the morning.

Subtracting the time it would take a new cluster to grew to 3 nm size (t_{growth}), and using growth rates reported by Kulmala et al. (2001), the comparison between t_{turb} and the actual time of nucleation t_{nuc}, see Fig. 5a, produces a similar correlation between t_{turb} and $t_{3\,\mathrm{nm}}$ or t_{nuc} ($r = 0.93$ and 0.94, respectively), however, the slope becomes closer to one and the zero bias was reduces for t_{nuc} compared to $t_{3\,\mathrm{nm}}$.

In fact, considering the time resolution of the SODAR profiles (30 min) and the DMPS system (10 min), t_{nuc} were significantly different from t_{turb} for only two cases (see Fig. 5a). We have also considered the convective time scale t^*, as this indicates how long time it would take for a tracer to be well mixed through the mixed layer. We did not have soundings close enough to the onset of nucleation to define t^* for more than a few of the cases in Fig. 5a, however, t^* did not change very much and averaged only 13 minutes, always smaller than t_{growth}, so even if we would subtract also t_{growth} from $t_{3\,\mathrm{nm}}$ the general pattern in Fig. 5a would change very little.

It could be that the relationship between t_{turb} and t_{nuc} in Fig. 5a is an indirect effect caused by

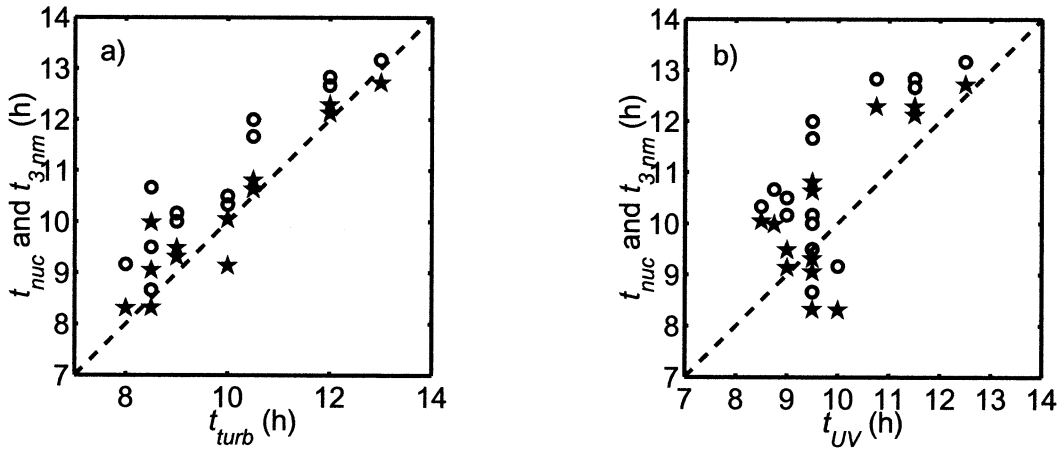

Fig. 5. (a) The time of onset of strong vertical wind variance as seen by the SODAR (the vertical component of the turbulent kinetic energy) related to the time of onset observation of 3 nm diameter particles (circles) and estimated time of nucleation (pentagram). The dashed line marks the 1:1 relationship. (b) The time of onset of strong UV-B radiation related to the time of onset observation of 3 nm diameter particles (circles) and estimated time of nucleation (pentagram).

the increasing incoming solar radiation, the enhancement of the OH production during the morning hours a sunny day. The sunlight will cause both more turbulence along with more OH production, consequently, it is very difficult to determine which has a dominating effect, or if both processes were of similar importance for the onset of nucleation. To test this, we have prepared Fig. 5b. Like turbulent kinetic energy, ultraviolet radiation (UV-B) increase rapidly in the morning, in practice, almost like a step function. We call the time of the most rapid increase in UV-B t_{UV} and compare it in Fig. 5b with t_{3nm} and t_{nuc}. The correlation between t_{UV} and t_{3nm} or t_{nuc} is much lower than between t_{turb} and t_{3nm} or t_{nuc}. There is still a general trend that nucleation occurs later on days with a cloudy morning (the four cases with $t_{UV} > 10{:}30$ in Fig. 5b), which delayed both the boundary layer evolution and the photochemistry. The days when nucleation started late, the increase in UV-B was also late, but the data does not line up so nicely on the 1:1 line as for turbulence. For the rest of the nucleation days, there is no relationship at all between t_{UV} and t_{3nm} or t_{nuc}. On days when t_{UV} was early, between 8:30 and 10, t_{3nm} and t_{nuc} are scattered randomly between 8 and 12. It appears that it is more likely that the increase in turbulence in the morning controls the onset of nucleation than that the increase in photochemistry occupies this key role.

3.3. Turbulent energy

We have systematically divided eddy-covariance fluxes and SODAR measurements into 3 categories.

(a) Days with cold air outbreaks and nucleation (4, 0, 11 days on BIOFOR 1, 2, 3, respectively).

(b) Days with cold air outbreaks, but no nucleation (6, 9 and 12 days on BIOFOR 1, 2, 3, respectively).

(c) Days without cold air outbreaks (which is always without nucleation). This includes days with warm air advection, no significant advection at all and with weak cold air advection. (22, 31 and 18 days on BIOFOR 1, 2, 3, respectively)

This allows us to examine if there are significant differences between these groups.

It can be seen from Fig. 6 that the surface layer sensible heat flux ($\overline{w'\theta'_0}$), as measured with the eddy covariance system, increased more rapidly

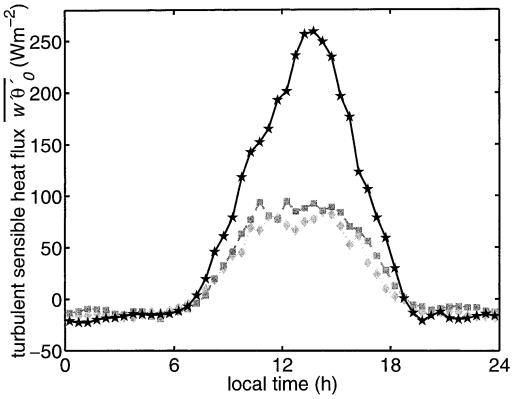

Fig. 6. BIOFOR 3 diurnal cycles of mean sensible turbulent heat fluxes in the surface layer for nucleation days (full black line with pentagrams), cold air advection days without nucleation (dashed gray line with squares) and the remaining days (dotted light gray line with diamonds).

and reached about a factor two higher values on nucleation days than on days without nucleation. This applies to all days without nucleation, independent on if there were cold air advection. Also the wind variances and temperature variance was larger in the surface layer during nucleation days. As the entrainment flux at the top of the mixed layer (e.g., $\overline{w'\theta'}(z_i)$ for sensible heat) is proportional to the surface flux (Stull, 1976), this suggests that also the entrainment fluxes, and the turbulent fluctuations they cause, was significantly stronger during the nucleation days. Fig. 7 shows the average turbulent kinetic energy in vertical (σ_w) and horizontal (σ_u) components up to 500 m as measured by the SODAR for the nucleation days and for days with cold air advection but no nucleation. In either case σ_w and σ_u were larger in daytime than in nighttime, but the turbulent kinetic energy was on average a factor two larger on nucleation days, both compared to days with similar synoptic settings and to days with different weather situations, no cold air advection (not shown). One can also see how a maximum in vertical wind variance developed in the upper part of the SODAR range on nucleation days, owing to stronger vertical convective up drafts, in agreement with mixed layer similarity theory. Since cold air outbreak days without nucleation resemble any day without advection, this suggests that turbulence, convection and entrainment were

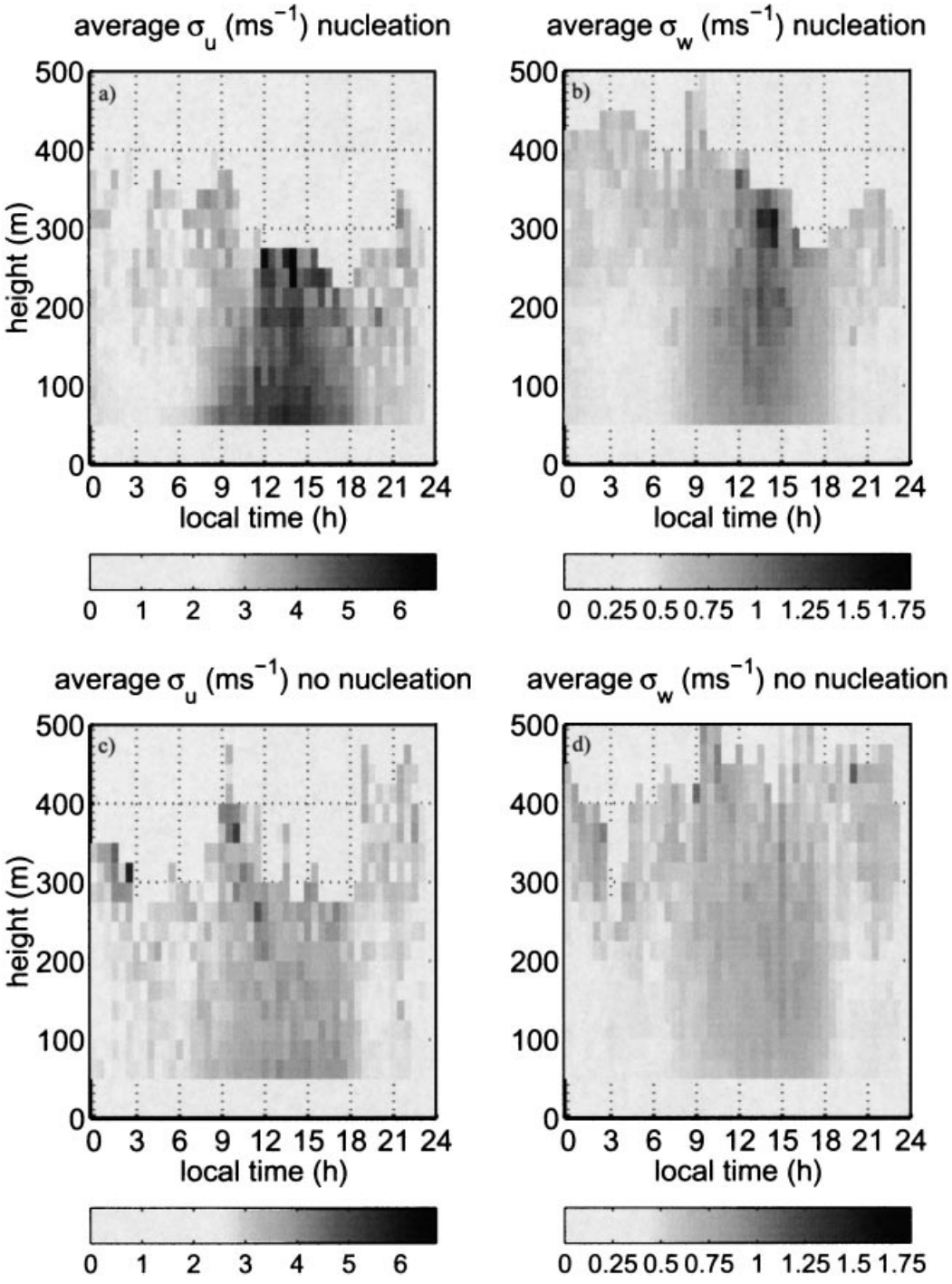

Fig. 7. (a) BIOFOR 3 average diurnal variation in vertical profiles horizontal wind standard deviation for days with nucleation, in cold air outbreaks. (b) Vertical wind standard deviation for days with nucleation, in cold air outbreaks. (c) Horizontal wind standard deviation for days without nucleation, in cold air outbreaks. (d) Vertical wind standard deviation for days without nucleation, in cold air outbreaks.

key processes for the nucleation, along with photochemical processes (Kulmala et al., 2001; Jansson et al., 2001). It may even help explaining why some cold air outbreak days resulted in nucleation and others didn't.

3.4. Boundary layer growth and entrainment

In Fig. 3 the simulated BL growth was presented on 4 April 1999. It was a case of calm night preceding the nucleation event, with low turbulence intensities (friction velocity from 0.1 to 0.2 ms^{-1}) and a strong temperature inversion formed during the night, see Fig. 2. The 3-nm particles were observed close to the surface at about 10:10, which indicates nucleation at about 9:20 if one takes into account the growth from stable cluster to 3 nm diameter. That would be right in the middle of the most rapid growth of the mixed layer through the residual layer, see Table 1. The following night, however, was windy and partly cloudy with significant mechanically generated turbulence present (night-time friction velocity values between 0.4 and 0.5 ms^{-1}). As a result, the near-surface layer was mechanically mixed up to a few hundred meters, enabling turbulent transport of near-surface properties to higher layers. Again the evolution of the mixed layer height agrees well with observation (not shown). The nucleation mode particles appeared around 9:30, which corresponds to a nucleation starting at about 9:00, see Table 1. That was only half an hour after the onset of strong turbulence according to the SODAR, but before the fast mixed layer growth and high entrainment velocities according to the simulation. In fact, during the fast growth of the mixed layer from 10:00 to 12:30, the aerosol number decreases (not shown).

All together there are 6 nucleation days when soundings were performed in Hyyhälö, all during the BIOFOR 3 campaign. Three of these days were preceded by nights with significant turbulence and three with low turbulence conditions. Table 1 summarizes the simulated mixed layer heights for the time when nucleation mode particles were observed. The table indicates that by the time nucleation started, there was always a mixed layer. This implies that mixing of the near-surface air with the air from stable layer above or the residual layer had occurred. After the calm night when nucleation started, the mixed layer height at the observation of nucleation ($t_{3\,nm}$) was generally higher than after the turbulent night and the growth was faster and more pronounced. After the calm night the nucleation mode particles appeared always during or right after the fast mixed layer growth and large entrainment, e.g., Figs. 3, 4. After the more turbulent nights the nucleation started before the fast growth of the mixed layer through the residual layer. However, since the nucleation always started in connection to the onset of strong turbulence, a more shallow convection and moderate entrainment must have started.

After a calm stable stratified night, the nocturnal inversion must first be consumed by the solar heating and the stratification must become neutral before the strong turbulence can start. After a more turbulent night (which might have had higher winds or cloud cover) the stratification near surface is already near neutral, or much less stable, at sunrise. Hence, strong turbulence can form

Table 1. *Onset of nucleation and turbulence, period of largest mixed layer growth and strongest entrainment, estimated mixed layer heights by the time of approximate beginning of nucleation event; the table also indicates the turbulent conditions during the previous night and the earliest possible time of entrainment from the free troposphere (FT)*

Day in 1999	Previous night	$t_{3\,nm}$	t_{nuc}	t_{turb}	Growth period	Earliest FT	z_i (m)
30March	turbulent night due to front passage	09:10	8:20	8:00	11:30–14:00	never	290
4 April	calm night	10:10	9:20	9:00	9:00–9:40	9:40–13:00	1490
5 April	turbulent, windy and cloudy night	09:30	9:00	8:30	10:00–12:30	13:00–never	490
8 April	calm night	12:50	12:20	12:00	12:30–14:10	14:10–14:30	820
12 April	turbulent night due to low level jet	10:10	9:30	9:00	9:30–11:50	14:30–never	600
13 April	calm night	10:30	9:10	10:00	9:00–10:20	11:00–12:20	1010

earlier and convection will start already in this initial mixed layer. The maximum entrainment fluxes may not occur at the same time as the maximum w_e since the entrainment is also a function of the gradient over the entrainment zone, e.g., $\Delta_{EZ}\overline{\theta}$ for the entrainment heat flux. c.f. Fig. 3b,e. Usually, $\Delta_{EZ}\overline{\theta}$ as well as the water vapor gradient were larger in the early development of the mixed layer than during the fastest growth of the mixed layer, c.f. Fig. 2. In fact, part of the explanation to the fast growth is that the temperature difference between the mixed layer and the residual layer becomes very small. For example, our simulations for 5 April showed a rapid decrease in $\Delta_{EZ}\overline{\theta}$ from 9–11:00 and values close to zero from 11–12:00, and as w_e had a maximum when $\Delta_{EZ}\overline{\theta}$ had a minimum, the actual $\overline{w'\theta'}(z_i)$ was more constant. This will probably apply also to the gases and aerosols in the way that their actual entrainment would reach a maximum earlier than w_e.

In all cases, entrainment from free atmosphere occurred too late to be the cause of the observation of 3-nm particles. Therefore, if entrainment of ultrafine particles or clusters caused the appearance of 3-nm particles, it must have been entrainment from the residual layer. On the other hand, on 5 April, the period of largest entrainment from the residual layer caused the aerosol number to decrease by 13,000 cm^{-3}, as if dilution of the mixed layer air overwhelmed nucleation for a while.

3.5. *Evolution of the aerosol size distribution during the late morning entrainment*

It was often observed during the mixed-layer formation and growth after sunrise that the particle number in the Aitken and/or accumulation modes decreased significantly, e.g., Fig. 4b. This behavior was observed on approximately one third of the nucleation days, usually such that the Aitken and accumulation mode particles were reduced a short period before the appearance of nucleation mode particles. The decrease in concentration coincides with the mixed layer growth and was probably caused by dilution of high particle concentrations in the mixed layer with the entrained air. Measured aerosol number size spectra have been analyzed by fitting 2 or 3 (depending on the concentration of smallest particles) lognormal modes to the particle size spectra. The concentration for each mode (nucleation, Aitken and accumulation modes) was calculated. The Aitken mode had an average diameter of 46 nm and the accumulation mode averaged 160 nm in modal diameter (Aalto et al., 2001).

Under the conditions of negligible horizontal advection, the mixed layer aerosol concentration can be described by

$$\frac{dC_{ML}}{dt} = \frac{w_E}{z_i} C_E - \frac{w_E + v_d}{z_i} C_{ML}, \tag{3}$$

where C_E is the concentration in the entrained air and v_d is the dry deposition velocity. If to assume that the entrained concentration is constant for the period of analysis, the time evolution of the mixed layer concentration is given by

$$C_{ML}(t) = C_{ML}(t_0)\exp\left(\int_{t_0}^{t}\frac{w_E + v_d}{z_i}\,dt\right) + C_E\left\{1 - \exp\left(\int_{t_0}^{t}\frac{w_E + v_d}{z_i}\,dt\right) \times\left[1 + \int_{t_0}^{t}\frac{v_d}{z_i}\exp\left(\int_{t_0}^{t}\frac{w_E + v_d}{z_i}\,dt\right)dt\right]\right\}.$$

The integrals in the above equation can be calculated from modeled entrainment velocities and mixed layer heights, as in Fig. 3, assuming deposition velocity value (deposition affects only marginally the mixed layer concentration evolution). Then, the ML concentration C_{ML} at some initial time moment t_0 and entrained concentration C_E can be obtained from regression of above equation to measured concentration time series.

Fig. 8a shows the time evolution of Aitken mode concentration as determined from particle size spectrum and presented by above equation on 3 April 1999. Deposition velocity was assumed to be 10^{-3} ms^{-1} and sensitivity tests revealed only little effect of deposition velocity on concentration. Figs. 8b,c give the Aitken and accumulation mode concentration series for 4 April and 12 April 1999, respectively. The good qualitative agreement of the concentration evolution indicates that entrainment is the main process responsible for the concentration decrease and also that the mixed layer height and entrainment velocity simulation represent the mixed layer growth well.

Table 2 contains the estimated modal concentrations of particles in the mixed layer at the

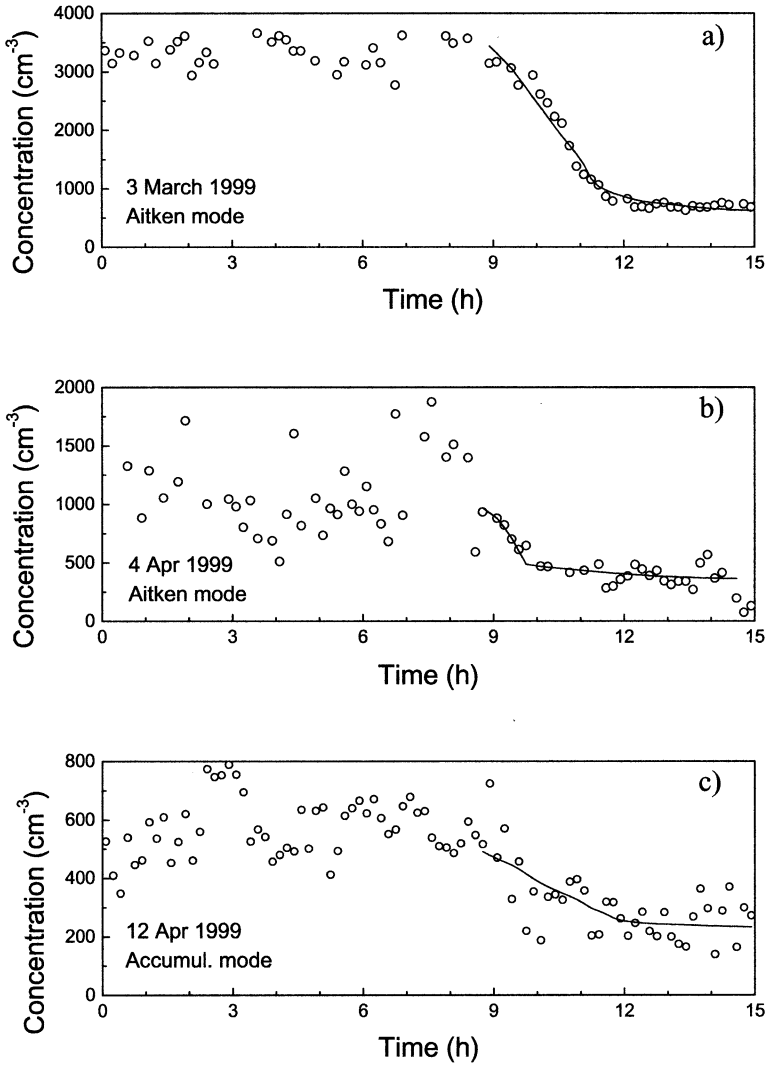

Fig. 8. (a) Measured (circles) and modeled (line) Aitken mode number concentration during 3 April 1999. (b) 4 April, (c) 12 April and the accumulation mode.

Table 2. *The ML modal particle concentrations at given times and estimated average concentrations in entrained air; the errors are 3 standard deviations of the concentration estimates (confidence level 0.997)*

Day in 1999	t_0	Mode	$C_{ML}(t_0)$ (cm^{-3})	C_E (cm^{-3})
3 April	08:27	Aitken	3740 ± 400	-59 ± 75
4 April	08:26	Aitken	1020 ± 280	207 ± 46
4 April	08:26	accumul.	830 ± 220	-170 ± 35
12 April	08:36	Aitken	1040 ± 540	379 ± 101
12 April	08:36	accumul.	500 ± 230	142 ± 43

beginning of each growth simulation together with the average concentration of entrained air, which explains the observed concentration behavior in the mixed layer. The estimated Aitken mode particle concentration on 3 April in the residual layer is negative, but not significantly different from zero. However, on 4 April the estimated accumulation mode concentration in entrained air was negative, although the fit of concentration time series was very good (not shown). The estimated negative concentration is a result of conditions not satisfying the assumptions. Eq. (3) and consequently eq. (4) assume horizontal homogeneity, which might be violated in some cases. Furthermore, dividing the aerosol spectrum into Aitken and accumulation modes may cause artifacts if the modes drift in size. Table 2 also summarizes that the Aitken and accumulation mode particle concentrations above the mixed layer, in the residual layer and free troposphere, were significantly lower than inside the mixed layer on these nucleation days.

The strong reduction in aerosol number in the initial mixed layer growth may itself be an important factor for the onset of nucleation as it will rapidly reduce the condensational sinks in the mixed layer. If we assume that the nucleation occurred in the mixed layer and that the nucleation mode concentration was small aloft, the nucleation mode number will also experience dilution. This is difficult to study, owing to the strong simultaneous production of nucleation mode particles. In some cases, however, dilution by entrainment overwhelmed the production, which appears to have been the case on 5 and 12 April. Furthermore, the dilution must be considered when trying to estimate the nucleation rate from observed number increase. Only if the nucleation rate is constant through all of the mixed layer during the growth will the observed number increase correspond directly to the actual nucleation rate (for the moment neglecting coagulation and deposition sinks).

3.6. *Turbulent aerosol number fluxes near surface on nucleation days*

On 12 April 1999, during BIOFOR 3, the nucleation started at about 9:30 local time. Fig. 9 show the evolution of the surface layer turbulent aerosol number flux. After a night and morning with downward aerosol fluxes, two data points show upward fluxes (8:30 and 9:30). This was a frequent feature on days when the decrease in Aitken and accumulation mode number concentrations due to entrainment from the residual layer was so rapid that there were an upward flux from the air close to the surface. From 9:30 to 10, the aerosol flux changed sign to rapidly increasing downward fluxes and reached a maximum level from noon until the evening, but with large fluctuations on a time scale of 1–2 h. The large downward flux during the nucleation event is typical for the nucleation days (87% of the cases, see Buzorius et al., 2001), which support the concept of an elevated source, above the canopy and the surface layer, for the new particles. The fluctuations in the afternoon was also a very common feature indicating a variability on a time scale just below the half hour averages of turbulent aerosol fluxes. Frequently, but not always, this coincided with the appearance of cloud streets on satellite images, indicating the formation of roll vortices in the fully developed convective mixed layer (Nilsson et al., 2001). Roll vortices have been reported to change both aerosol concentration (Bigg et al., 1996) and fluxes (Smedman, 1991) periodically at a fixed point at the surface. This results from a small angle between the roll axes and the mean wind direction, which causes them to drift slowly over the surface creating periodicity's on this time scale in radiation, fluxes and concentrations as the cloud streets and up or down draft regions of the rolls passes over the point of observation. Buzorious et al. (2001) showed that the periodicity is best seen in the low frequency spectral peak in the cross wind component with an energy maximum at 20 min. Periods of enhanced momentum fluxes was accompanied by increased sensible and latent heat fluxes and larger downward aerosol fluxes.

3.7. *Conserved variable mixing diagram analysis*

In Subsections 3.5, 3.6, we have been able to exclude the canopy and the free troposphere as the origin of the new particles. To decide where in between (the mixed layer, the entrainment zone or the residual layer, c.f. Fig. 1) the nucleation occurred in-situ measurements throughout the depth of the boundary layer are really required. We can, however use conserved variable mixing

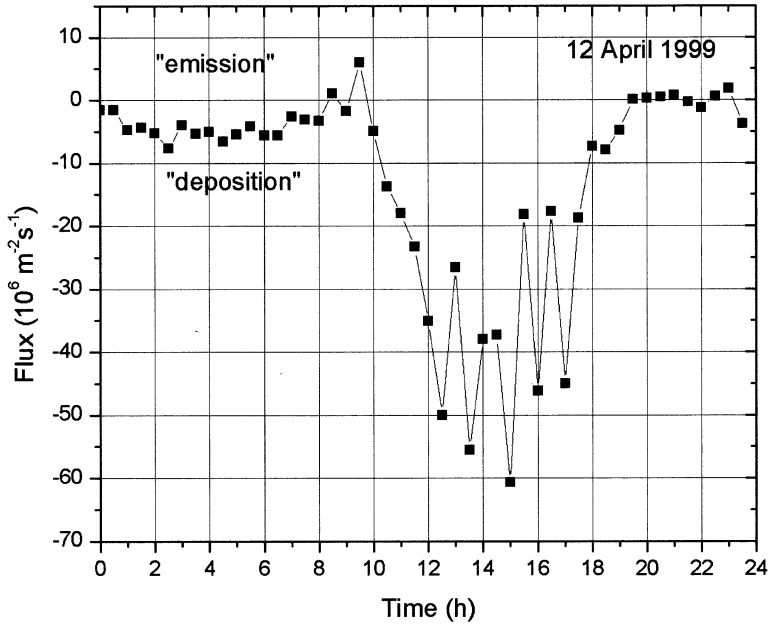

Fig. 9. Turbulent aerosol number flux in the surface layer above the canopy as measured with the eddy covariance flux system in the Hyytiälä mast through 12 April 1999 (BIOFOR 3).

diagram analysis which previously has been used effectively to elucidate boundary layer dynamics and entrainment processes in cumulus clouds (Lenschow et al., 1999). When there is no net flux of a variable to or from a parcel, and that variable does not undergo any loss or gain processes, then it is said to be a conserved variable. In meteorological terms, conserved variables are typically total water content and wet equivalent potential temperature (θ_v). If we take a stratified part of the atmosphere with two adjacent layers each possessing distinct thermodynamic properties with no mixing between them, and plot a scatter plot of water content and potential temperature, two clusters, corresponding to the two distinct thermodynamic states will result. If, however, mixing between the two layers occurs, a linear mix of both thermodynamic states will be located on a line, with a non-zero slope, between the two clusters representing the two initial layers in a scatter plot. The distance from one cluster corresponds directly to the degree of mixing with the parcel represented by that cluster. Conversely, if a variable is not conserved within one layer, then a line extruding out of one of the clusters, with a zero slope will result, as one variable will vary independently of the other. We can utilize both of these concepts to elucidate whether or not particles are formed in-situ or whether they are simply entrained from another layer.

Six nucleation and growth event cases were analyzed using this technique during BIOFOR 3. Although we were not able to conduct a vertical profile of aerosols through the boundary layer, we can assume, due to the presence of boundary layer circulations, that measurements at one point in the mixed layer corresponds to similar sampling that would result from a profile through that layer. Furthermore, we can use the profiles of temperature and water vapor from the radio sonds to help understanding what vertical level vertically mixed air originated from. The choice of conserved variables is difficult since there is, mostly, some exchange of water and heat in the surface layer. For the environment in question, it was found that the temperature change caused by turbulent heat flux was significantly higher than the difference between different layers and, consequently, potential temperature could not be used as a conserved variable. On the other hand, water vapor (Q) fluxes were found to be negligible compared to the water vapor concentration in the air,

as was the case for CO_2. Thus, we are able to treat water content and CO_2 as conserved variables.

On 8 April, there was initially little variation in the values of Q or CO_2 and both the early time periods in Fig. 10a are seen to converge around clusters corresponding to concentration of 6.4–6.7 g kg^{-1} and 378–380 ppb, respectively. During the 3rd period of Julian Day 98.48–98.53 (11:31–12:43) a mixing line converged on the state of the 4th period, Julian Day 98.53–98.56 (12:43–13:19), corresponding to a CO_2 concentration of 371–374 ppb and a water contend of 3.6–4.6 g kg^{-1} (see Fig. 10a). This new stable cluster of points, suggests that the boundary layer had, at this stage, become well mixed and reached a new thermodynamic state. The initial observed water gradient over the entrainment zone (ΔQ_{EZ}) was large. The same applies to the initial vertical temperature gradients and the vertical CO_2 gradient must also have been large to explain the appearance of the diagonal mixing line in Fig. 10a. A mixing line in Fig. 10b from 4.6 to 4.2 g kg^{-1} and 1600 to 2000 cm^{-3} corresponds to the early part of the 4th period in Fig. 10a, approximately at the onset of strong entrainment and mixed layer growth. A comparison with Q from the sonde data indicates that the initial nucleation occurred in the entrainment zone. However, nucleation continued throughout the period of mixed layer growth and caused a large increase in aerosol number concentration up to $\sim$8000 cm^{-3} and a gradually decreasing Q with much less slope (from 4.2 to 4.6 g kg^{-1}), which could indicate in-situ nucleation in the now much deeper mixed layer. However, as both ΔQ_{EZ} and $\Delta\theta_{EZ}$, and probably most other vertical gradients, had been reduced to small numbers by that time, like for 4 April in Fig. 2, we cannot exclude that the later nucleation still occurred in the entrainment zone or residual layer.

For example, on 4 April 1999, it appears that nucleation occurred in the entrainment zone during the most intense period of mixed layer growth and entrainment, as the appearance of 3 nm particles were associated with Q and θ values representative of the entrainment zone. Especially for Q and N there were a clear mixing line, with a scatter much smaller than ΔQ_{EZ}. On the other hand, the nucleation on, e.g., 12 April must have occurred in the mixed layer, entrainment zone or residual layer during the early stage of the mixed layer growth. We cannot say which one from the mixing diagrams since the observed ΔQ_{EZ} and $\Delta\theta_{EZ}$ were both very small (the later approached zero from 9:00 to 11:00 according to the mixed layer growth model). However, during the period of most rapid increase in z_i and largest w_e (11–11:50), the concentration of ultrafine aerosol particles actually decreased by about 2000–3000 cm^{-3}. This could be explained by dilution of the mixed layer nucleation mode aerosol similar to that demonstrated for the Aitken and accumulation modes in Subsection 3.5. Indirectly, this supports in-situ nucleation in the mixed layer or implies that if there was a flux of aerosol particles from aloft, they must have been less than 3 nm and the growth must have occurred in the mixed layer. In all cases the free troposphere may be excluded as the source of the new particles.

4. Discussion and conclusions

As reported by Nilsson et al. (2001), the nucleation occurred in Arctic and polar air masses during cold air outbreaks. The clear sky continental boundary layer typical for these synoptic conditions favors large amplitudes in boundary layer depth and fluxes. In particular, the transition is violent when the morning mixed layer breaks through the nocturnal stable boundary layer. In a few hours, convection and entrainment grow the convective mixed layer an order of magnitude deeper than the nocturnal boundary layer. We have found these processes to be more pronounced and powerful on nucleation days and to be strongly correlated to the aerosol nucleation. The smallest detectable particles (3 nm) occurred within 10 minutes to 2 hours from the onset of strong turbulent energy. This was equally true for boundary layers that made this transition in the morning, around noon or in the early afternoon. When considering the time it will take for the new nanometer sized aerosol to grow to 3 nm, the relation between nucleation and turbulence onset were even stronger. Turbulent sensible heat fluxes in the surface layer and turbulent kinetic energy in the lower mixed layer were twice as high on nucleation days compared to other days. Since the entrainment fluxes are driven by overshooting convective plumes is the heat flux at the top of

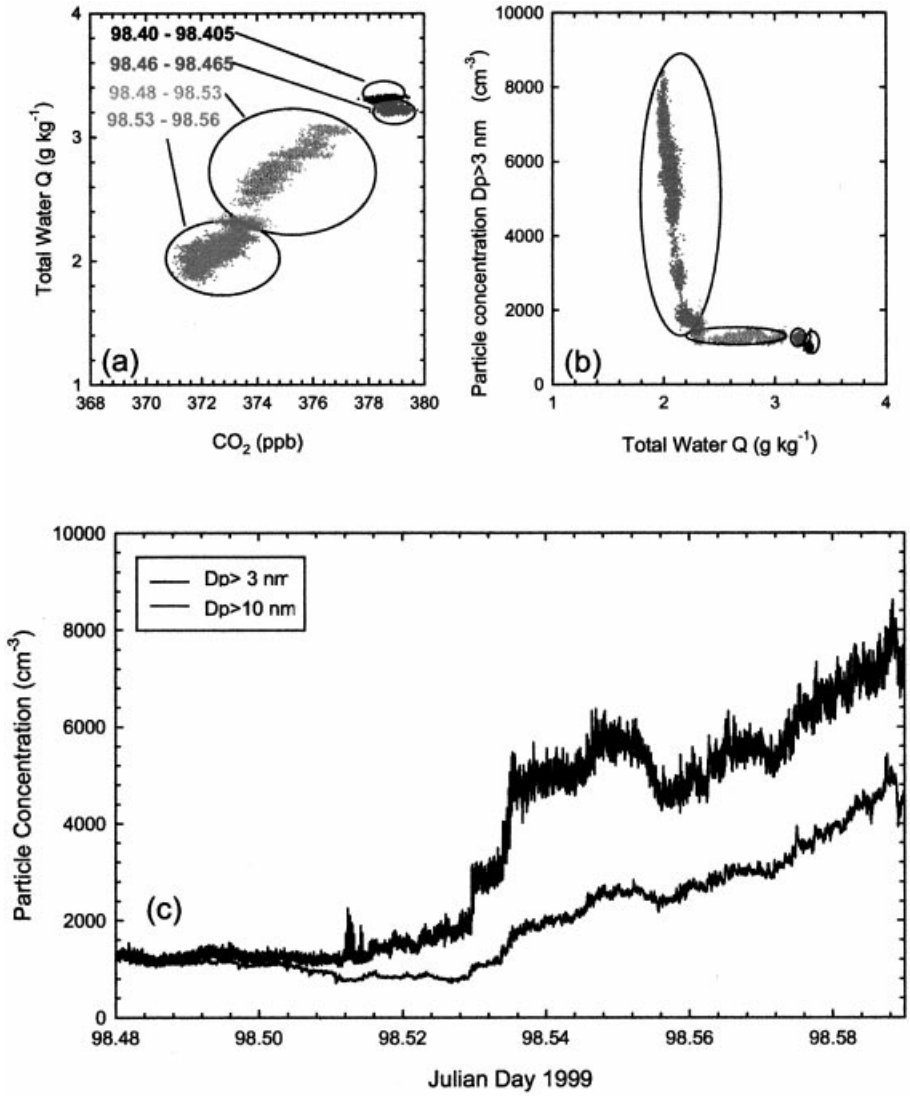

Fig. 10. (a) Conserved variable mixing diagram for 8 April 1999, BIOFOR 3 of CO_2 and total water by four different periods before and during the nucleation event. (b) Total water and aerosol number concentrations ($D_p > 3$ nm). (c) Particle number concentration for $D_p > 3$ and 10 nm (grey) for the same periods as in (a) and (b).

the mixed layer proportional to the surface layer flux. This suggests entrainment and convection as key process for the nucleation. The onset of strong turbulence in the morning sometimes coincided with (or caused) the period of the most rapid mixed layer growth. In other cases, the rapid mixed layer growth started later than the strong turbulence. Based on just six cases, this appears to be related to the initial conditions and turbulence and static stability during the previous night. In either case, the nucleation occurred at the same time as the onset of strong turbulence (based on 15 cases), which indicates that the deeper convection is not required to cause the nucleation, but turbulence in the early mixed layer, and associated entrainment seems sufficient to induce nucleation. It also appears that the onset of turbulence in the morning was better correlated with the onset of

nucleation than the onset of photochemical production of precursor gases for the nucleation, although both processes have an increasing trend during the morning hours.

Large downward turbulent aerosol number fluxes in the surface layer during each nucleation day exclude the possibility that the nucleation occurred below the eddy covariance system, in the canopy. Both the mixed layer growth simulations and the conserved variable mixing diagrams excludes the possibility of entrainment fluxes from the free troposphere, which were not important until after the nucleation events. Although based on only a few cases, it appears that the most likely site for nucleation in the vertical structure are either or both the mixed layer, the entrainment zone, or the residual layer as an open possibility, while the surface layer and the free troposphere can be excluded.

4.1. Formulating hypothesizes

The correlation between the onset of nucleation and the onset of turbulence, rather than the incoming solar radiation, suggests that there is a connection between boundary layer dynamics during this period and aerosol formation events. We can formulate several different hypothesizes which all could explain this. None of these hypothesizes is meant to question the fact that with the rising sun and increased solar flux, more OH will be produced, leading to the enhanced production of precursor vapors. Instead, these hypotheses are meant to explain that, concomitant with the production of precursor vapors, the onset of turbulence appears to be a pre-requisite to trigger nucleation.

(1) On the days when a dilution of the preexisting aerosol number and condensation sink was observed before the nucleation, this may itself be enough to trigger nucleation by decreasing the sink of precursor gases at the same time that the precursor production may be increasing due to increasing photochemical activity. Such a scenario would form favorable conditions for nucleation.

(2) If there was a sufficient concentration of vapor A present in the stable nocturnal layer, or in the early morning shallow mixed layer, but an insufficient concentration of vapor B for both species to nucleate, there would be no particle formation. However, if B or its precursor gases, were abundant (e.g., due to increased photochemical production) in the residual layer, entrainment of air into the mixed layer could cause the necessary concentrations of A and B to nucleate. For this to work, there must be a high concentration of vapor A originally, since the shallow early morning mixed layer is so heavily diluted.

(3) New particles or clusters had formed in the residual layer in large numbers due to increased photochemical activity, but because of low vapor pressures (including low water vapor pressure), these were unable to grow fast enough to detectable sizes before they were lost to coagulation. As they were entrained into the vapor rich mixed layer, they could grow rapidly to detectable sizes. The primary problem with this hypothesis is that it only relocates the problem. Owing to the small aerosol size and therefore short lifetime, we will instead have to explain how nucleation occurs in the residual layer. A version of this hypothesis which doesn't suffer from this problem can be built on the recent results of Kulmala et al. (2000), who suggests that ternary nucleation of water, sulfuric acid and ammonia efficiently form a dynamic population of thermodynamically stable sulphate clusters. The situation may very well be that there was insufficient condensable vapors in the residual layer for these clusters to grew to 3 nm, and so much preexisting aerosol in the stable boundary layer and early mixed layer that the clusters are lost by coagulation. Entrainment of residual layer air with low aerosol concentration into the vapor rich mixed layer could then cause perfect conditions for the thermodynamically stable sulphate clusters to grow to 3 nm and more.

(4) The nucleation rate is increased by adiabatic cooling in the rising convective air (Easter and Peters, 1994) and by the entrainment over the capping inversion (Nilsson and Kulmala, 1998) associated with this period of boundary layer evolution. It is reasonable to assume that the nucleation rate, independent of the nucleation pathway, would reach maximum values at the coldest place of the boundary layer, that is the top of the mixed layer or the maximum height of each rising convective plume. It is important to realize that the large entrainment fluxes at the top of the mixed layer causes large fluctuations in the temperature and relative humidity in and just below the entrainment zone. The temperature fluctuations will enhance the nucleation rate of

any nucleation path. Furthermore, the typically opposite temperature and humidity profiles, e.g., Fig. 2, at the top of the mixed layer cause temperature and humidity fluctuations to be anti-correlated (Lenschow and Wyyngard, 1980). For nucleation paths that include water vapor, such as binary homogeneous nucleation with $H_2O + H_2SO_4$, this will enhance the nucleation rate even more (Easter and Peters, 1994). It is the nature of convective mixed layers that the enhancement in nucleation rate by entrainment driven turbulent fluctuations would take place at the top of the mixed layer, which has the lowest average temperature, hence combining two powerful forces that favors nucleation. While the increasing solar radiation increases the production of, for example, H_2SO_4, the adiabatic cooling and turbulent fluctuations will enhance the nucleation so that the onset of significant nucleation will occur earlier, thereby controlling the time at which the aerosol nucleation become significant.

The convective roll vortices observed by Buzorious et al. (2001) would probably be the most powerful manifestation of convection, which could efficiently drive air parcels through cycles of adiabatic cooling and cause enhanced nucleation at the top of the updraft regions of the roll vortices. Periodicity in momentum and heat fluxes were observed before the nucleation mode particles were observed, thus the convection and adiabatic cooling they caused may have been involved in the initiation of the aerosol formation processes. The roll vortices may also be of large importance for the growth of the aerosol and they may cause the first cloud processing of the new aerosol.

All these hypothesizes allow the time delay of 10 min to 2 h to be explained by growth to the detection limit of 3 nm and by the time needed for transport from an elevated source to the surface. More than one of these effects may have worked together, or where one of them may be critical for one nucleation event, another may have been most important for the next nucleation day. Without the driving force of any of these processes, nucleation may still occur driven by photo chemistry only, but probably on less days and at a later time of the day. Which is the dominant effect may change between different sites and periods. Even if none of these hypotheses are correct, the strong entrainment during the nucleation periods has to be considered. The near-surface air is diluted approximately one order of magnitude with air from aloft, which will influence the sequence leading to nucleation as well as any attempts to estimate the nucleation rate from observed aerosol numbers.

5. Acknowledgements.

The European Commission (Contract ENV4-CT97-0405) financed the BIOFOR project. The lead author would like to thank the Wenner-Gren Center Foundation and the Swedish Natural Science Research Council (contract G-AA/AS 11858–302 and G-AA/GU 11858–303) for financial support.

REFERENCES

Aalto. P., K. Hämeri, E. Becker, R. Weber, J. Salm, J. Mäkelä, M. Väkevä, I. Koponen, H. Karlsson and C. Hoell, 2001. Aerosol physical properties of aerosol particles during nucleation events. *Tellus* **53B**, 344–358.

Aubinet, M., Grelle, A., Ibrom, A., Rannik, Ü., Moncrieff, J., Foken, T., Kowalski, A. S., Martin, P. H., Berbigier, P., Bernhofer, Ch., Clement, R., Elbers, J., Granier, A., Grünwald, T., Morgenstern, K., Pilegaard, K., Rebmann, C., Snijders, W., Valentini, R. and Vesala, T. 2000, Estimates of the annual net carbon and water exchange of European forests: the EUROFLUX methodology. *Adv. Ecol. Res.* **30**, 113–175.

Bigg, E. K., Leck, C. and E. D. Nilsson, 1996. Sudden changes in arctic atmospheric aerosol concentrations during summer and autumn. *Tellus* **48B**, 254–271.

Birmilli, W. and A. Wiedensohler, 2000. New particle formation in the continental boundary layer: Meteorological and gas phase parameter influence. *Geophys. Res. Let.* **27**, 3325–3328.

Birmilli, W., A. Wiedensohler, C. Plass-Dülmer and H. Berresheim, 2000. Evolution of newly formed aerosol particles in the continental boundary layer: a case study including OH and H_2SO_4 measurements. *Geophys. Res. Let.* **27**, 2205–2208.

Buzorius, G., Rannik, Ü., Mäkelä., J. M., Keronen, P., Vesala, T. and Kulmala, M. 2000. Vertical aerosol fluxes measured by the eddy covariance method and deposition of nucleation mode particles above a Scots pine forest in southern Finland. *J. Geophys. Res.* **105**, 19,905–19,916.

Buzorius, G., Û. Rannik, E. D. Nilsson and M. Kulmala,

2001. Vertical fluxes and micrometeorology during aerosol particle formation events. *Tellus* **53B**, 394–405.

Coe, H., P. I. Williams, G. McFiggans, M. W. Gallagher, K. M. Beswick, K. N. Bower and T. W. Choularton, 2000. Behaviour of ultrafine particles in continental and marine air masses at a rural site in the United Kingdom. *J. Geophys. Res.* **105**, 26,891–26,905.

De Reus, M., J. Ström, M. Kulmala, L. Pirjola, J. Lelieveld, C. Schiller and M. Zöger, 1998, Airborne aerosol measurements in the tropopause region and the dependence of new particle formation on pre-existing particle number concentration. *J. Geophys. Res.* **103**, 31,255–31,263.

Easter, R. C. and L. K. Peters, 1994. Binary homogeneous nucleation: temperature and relative humidity fluctuations, non-linearity and aspects of new particle production in the atmosphere. *J. Appl. Meteorol.* **33**, 775–784.

Korhonen, P., Kulmala, M., Laaksonen, A., Viisanen, Y., McGraw, R. and Seinfeld, J. H. 1999, Ternary nucleation of H_2SO_4, NH_3 and H_2 in the atmosphere. *J. Geophys. Res.* **104**, 26,349–26,354.

Kulmala, M., A. Toivonen, J. M. Mäkelä and A. Laaksonen, 1998. Analysis of the growth of nucleation mode particles observed in Boreal forest. *Tellus* **50B**, 449–462.

Kulmala, M., Pirjola, L. and Mäeklä, J. M. 2000. Stable sulfate clusters as source of new atmospheric aerosol particles. *Nature*, **404**, 66–69.

Kulmala, M., K. Hämeri, P. P. Aalto, J. M. Mäkelä, L. Pirjola, E. D. Nilsson, G. Buzorius, Ü. Rannik, M. Dal Maso, W. Seidl, T. Hoffmann, R. Janson, H.-C. Hanssin, C. O'Dowd, Y. Viisanen and L. Laaksonen, 2001a. Overview of the international project on Biogenic aerosol formation in the boreal forest (BIOFOR). *Tellus* **53B**, 327–343.

Kulmala, M., P. Korhonen, L. Laakso and L. Pirjola, 2001b. Nucleation in boreal forest boundary layer. *Env. and Physics Chem.*, in press.

Lenschow, D. H. and J. C. Wyngaard, 1980. Mean-field and second-momentum budgets in baroclinic, convective boundary layer. *J. Atmos. Sci.* **37**, 1313–1326.

Lenschow, D. H., I. R. Paluch, A. R. Bandy, D. C. Thornton, D. R. Blake and I. Simpson, 1999. Use of a mixed-layer model to estimate dimethylsulfide flux and application to other traces gas fluxes. *J. Geophys. Res.* **104**, 16,275–16,295.

Mäkelä, J. M., P. Aalto, V. Jokinen, T. Pohja, A. Nissinen, S. Palmroth, T. Markkanen, K. Seitsonen, H. Lihavainen and M. Kulmala, 1997. Observations of ultrafine aerosol particle formation and growth in boreal forest. *Geophys. Res. Let.* **24**, 1219–1222.

Mäkelä, J. M., Dal Maso, M., Laaksonen, A., Kulmala, M., Pirjola, L., Keronen, P and Laakso, L. 2000. Characteristics of the aerosol particle formation events observed at a boreal forest site in southern Finland. *Boreal Env. Res.* **5**, 299–313.

Nilsson, E. D. and M. Kulmala, 1998. The potential for atmospheric mixing processes to enhance the binary nucleation rate. *J. Geophys. Res.* **103**, 1381–1389.

Nilsson, E. D., Pirjola, L. and Kulmala, M., 2000. The effect of atmospheric waves on aerosol nucleation and size distribution. *J. Geophys. Res.* **105**, 19,917–19,926.

Nilsson, E. D., J. Paatero and M. Boy, 2001. Effects of air masses and synoptic weather on aerosol formation in the continental boundary layer. *Tellus* **53B**, 462–478.

O'Dowd, C. D., G. McFiggens, L. Pirjola, D. J. Creasey, C. Hoell, M. H. Smith, B. Allen, J. M. C. Plane, D. E. Heard, J. D. Lee, M. J. Pilling and M. Kulmala, 1999. On the photochemical production of new particles in the coastal boundary layer. *Geophys. Res. Letts.* **26**, 1707–1710.

Pirjola, L., C. D. O'Dowd, I. M. Brooks and M. Kulmala, 2000. Can new particle formation occur in the clean marine boundary layer?. *J. Geophys. Res.* **105**, 26531–26546.

Smedman, A. 1991. Occurrence of roll circulations in a shallow boundary layer. *Boundary-Layer Meteorology* **57**, 343–358.

Stull, R. B. 1976. The energetics of entrainment across a density surface. *J. Atmos. Sci.* **30**, 1260–1267.

Stull, R. B. 1988. *An introduction to boundary layer meteorology*. 666 pp. Kluwer Academic, Boston, Mass, USA.

Väkevä, M., K. Hämeri, T. Puhakka, E. D. Nilsson, H. Hohti and J. M. Mäkelä, 2000. Effects of meteorological processes on aerosol particle size distribution in an urban background area. *J. Geophys. Res.* **105**, 9807–9821.

Zahn, A., C. A. M. Brenninkmeijer, M. Maiss, D. Scharffe, P. J. Crutzen, M. Hermann, J. Heintzenberg, H. Güsten, G. Heinrich, H. Fisher, J. W. H. Cuijpers and P. F. J. van Velthoven, 2000. Identification of extratropical two-way troposphere-stratosphere mixing based on CARIBIC measurements of O_3, CO, and ultrafine particles. *J. Geophys. Res.* **105**, 1527–1535.